Moiré-Induced Optical Nonlinearities: Single- and Multiphoton Resonances

A. Camacho-Guardian[1,*] and N. R. Cooper[1,2]
[1]T.C.M. Group, Cavendish Laboratory, University of Cambridge, JJ Thomson Avenue, Cambridge CB3 0HE, United Kingdom
[2]Department of Physics and Astronomy, University of Florence, Via G. Sansone 1, 50019 Sesto Fiorentino, Italy

(Received 17 August 2021; revised 14 October 2021; accepted 11 April 2022; published 20 May 2022)

Moiré excitons promise a new platform with which to generate and manipulate hybrid quantum phases of light and matter in unprecedented regimes of interaction strength. We explore the properties in this regime, through studies of a Bose-Hubbard model of excitons coupled to cavity photons. We show that the steady states exhibit a rich phase diagram with pronounced bistabilities governed by multiphoton resonances reflecting the strong interexciton interactions. In the presence of an incoherent pumping of excitons we find that the system can realize single- and multiphoton lasers.

DOI: 10.1103/PhysRevLett.128.207401

Introduction.—The ability to tune the optical, electronic, and transport properties in van der Waals heterostructures has opened the door for the engineering, realization, and detection of intriguing complex many-body phases of matter [1]. Much attention has focused on the electronic properties, which show novel quantum phases arising from strong interactions and provide a new test bed for quantum simulation [2,3]. However, these materials also hold interesting opportunities to study new hybrid quantum states of light and matter [4,5], and offer promising potential optoelectronic applications based on valleytronics [6–10] and twistronics [11].

In twisted bilayers of transition-metal dichalcogenides (TMDs) the emergent moiré periodicity [12–15] has significant effects on the nature of the excitons. In general these excitons are hybrids of the intralayer excitons formed by an electron and hole in the same layer and interlayer excitons with an electron and a hole belonging to different layers [16,17]. Hybrid excitons have attracted much attention as they possess tunable features of both intra- and interlayer character [18–20], and have strong mutual repulsion due to the dipole moment from their interlayer component.

In this Letter, we study the nature of the many-body states of *polaritons* formed by combining these strongly interacting hybrid excitons with a microcavity. We show that the optical nonlinearities arising from the interactions between the hybrid excitons can lead to features with no parallel in conventional two-dimensional polariton gases based on semiconductor quantum wells. When the cavity is driven coherently, the steady-state exhibits a bistability which, in contrast to two-dimensional polariton gases [21], is modulated by a discretized pattern, reminiscent of the equilibrium Mott insulating phase. When the excitons are pumped incoherently, we demonstrate that the strong correlations can cause the system to act as a *multiphoton* laser, akin to that of Rydberg and multilevel atoms [22–25]. In conventional semiconductor microcavities, most features —including the experimental realization of weakly interacting Bose-Einstein condensates [21,26,27], superfluid phases [28], and quantum vortices [29] of polaritons—can be understood in terms of weakly interacting polaritons described by the Gross-Pitaevskii equation, or other nonlinear classical description. Strong polariton-polariton interactions have been recently studied in the context of Feshbach polaritonic resonances [30,31], trion-mediated [32], and medium-induced optical nonlinearities [33–35]. However, to account for the physics of strongly interacting hybrid excitons in TMD bilayers [36], we must go beyond these works to consider the steady state properties of a Hubbard model of excitons coupled to a high-finesse cavity.

Model.—Consider a van der Waals heterostructure formed by two semiconductor monolayers, labeled A and B, coupled to a microcavity as shown in Fig. 1(b). For small twist angles, the lowest excitonic band acquires a hybrid character mixing intralayer and interlayer excitons [18]. In Fig. 1(a) we illustrate the relevant band configuration; intralayer excitons, in which the strong spin-orbit coupling makes the bands spin polarized at the points τK_A, are formed by an electron and a hole with spin fixed by the valley index τK_A ($\tau = \pm 1$) hybridize preferentially with interlayer excitons formed by τK_A electrons and $\tau' K_B$ holes with $\tau = \tau'$ for $K_A \simeq K_B$ [19]. We consider a single component $\tau = +1$, exploiting the valley-dependent selection rules, assuming that the light has circular polarization (σ^+) thus couples only to one valley. The properties of this band of hybrid excitons can be well described by a two-dimensional Bose-Hubbard Hamiltonian

$$\hat{H}_X = \sum_i \omega_X \hat{x}_i^\dagger \hat{x}_i + \sum_i \frac{U_X}{2} \hat{x}_i^\dagger \hat{x}_i^\dagger \hat{x}_i \hat{x}_i - \sum_{\langle i,j \rangle} t_{ij} \hat{x}_i^\dagger \hat{x}_j, \quad (1)$$

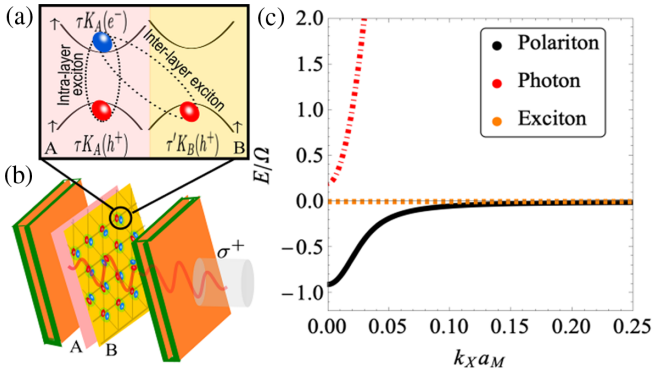

FIG. 1. (a) Band configuration of the intralayer and interlayer excitons. (b) Schematic representation of spatially localized hybrid excitons in a microcavity. (c) Enlargement of typical polariton, photon, and exciton dispersions, for $a_M = 5$ nm, $\Omega = 15$ meV and $m_c = 5 \times 10^{-5} m_e$, with m_e the electron mass.

where $\hat{x}_i^\dagger$ creates a $\tau = +1$ hybrid exciton in the Wannier orbital of the lowest band on site i. From now on we simply refer to this as an exciton. We consider N sites arranged on a triangular lattice with on-site energy ω_X, connected by the tunneling coefficients t_{ij}. The resulting band dispersion will not play a significant role in our results, since the local and repulsive interaction U_X will be assumed to be much larger than t_{ij}, as is typical for experimental systems [18].

The light-matter coupling is described by $\sum_{\mathbf{k}} \Omega(\hat{a}_{\mathbf{k}}^\dagger \hat{x}_{\mathbf{k}} + \hat{x}_{\mathbf{k}}^\dagger \hat{a}_{\mathbf{k}})$, where $\hat{a}_{\mathbf{k}}^\dagger$ ($\hat{x}_{\mathbf{k}}^\dagger$) creates a cavity photon (exciton) with in-plane momentum $\mathbf{k}$, and Ω is the Rabi coupling. (The photon is assumed to be circularly polarized.) The dispersion of free photons is $\hat{H}_l = \sum_{\mathbf{k}} \omega_c(\mathbf{k}) \hat{a}_{\mathbf{k}}^\dagger \hat{a}_{\mathbf{k}}$, with $\omega_c(\mathbf{k}) = \omega_c + |\mathbf{k}|^2/(2m_c)$, where m_c is the cavity photon mass.

The light-matter coupling only retains terms within the rotating wave approximation as the typical exciton energies (∼eV) are orders of magnitude larger than the Rabi coupling (∼meV). We assume, however, strong light-matter coupling, that is, we consider that the Rabi coupling Ω is much larger than the damping rate of the cavity photons, as commonly realized in exciton-polariton experiments [21]. As a consequence of the steep dispersion of light, Fig. 1(c), excitons couple to photons only within a very narrow region in momentum space $\Delta k a_M \lesssim \sqrt{2 m_c \Omega} a_M \approx 0.01$–$0.2$, with a_M the lattice constant of the moiré superlattice, typically of the order of $a_M \approx 1$–10 nm. The minimum wavelength $\lambda = 2\pi/\Delta k$ is thus orders of magnitude larger than a_M, such that $(\lambda/a_M)^2 \sim 10^3$–$10^5$, and a very large number of moiré sites couple collectively to the cavity field. This motivates a mean-field approximation (described below), in which the cavity is treated as a coherent state. Furthermore, we make the assumption—for uniformly driven systems—that the system retains translational symmetry, in which case there will only be significant occupation of the $\mathbf{k} = 0$ mode. We hereafter retain only this mode of the cavity field, which we now represent by $\hat{a}^{(\dagger)}$ without a momentum subscript, and take the cavity energy and light-matter interaction to be

$$\hat{H}_l + \hat{H}_{l-m} = \omega_c \hat{a}^\dagger \hat{a} + \frac{1}{\sqrt{N}} \sum_i \Omega(\hat{a}^\dagger \hat{x}_i + \hat{a} \hat{x}_i^\dagger). \quad (2)$$

Contrasting mobile two-dimensional excitons, saturation effects can become relevant at the level of a few excitons per site, underlining the quasizero dimensional nature of the local exciton states. While a full understanding of this phenomenon remains elusive [37,38], here for concreteness we account for this effect by adding an anharmonic light-matter coupling $\Omega(\hat{n}_i) = \Omega - \Omega_{\text{sat}} \hat{n}_i$, which prevents an arbitrarily large excitation number $\hat{n}_i = \hat{x}_i^\dagger \hat{x}_i$. Saturation effects are a reminder of the strictly nonbosonic nature of the excitons, relevant when the interparticle distance between the excitons is comparable to the exciton Bohr radius [39–41].

We account for intrinsic dissipative effects by studying the density matrix of the system, $\hat{\rho}$, whose time evolution is governed by the Lindblad master equation [21]

$$\frac{d\hat{\rho}}{dt} = -i[\hat{H}, \hat{\rho}] + \mathcal{D}[\hat{\rho}] = \mathcal{L}[\hat{\rho}], \quad (3)$$

where $\hat{H} = \hat{H}_X + \hat{H}_l + \hat{H}_{l-m}$. The dissipative natures of the cavity photons and the excitons are represented via the Lindblad operator

$$\mathcal{D}[\hat{\rho}] = \frac{\gamma_c}{2}[2\hat{a}\hat{\rho}\hat{a}^\dagger - \{\hat{a}^\dagger \hat{a}, \hat{\rho}\}] + \sum_i \frac{\gamma_x}{2}[2\hat{x}_i \hat{\rho} \hat{x}_i^\dagger - \{\hat{x}_i^\dagger \hat{x}_i, \hat{\rho}\}], \quad (4)$$

where γ_x and γ_c are the damping rates of the excitons and photons, respectively. We work in the regime where the linewidth of the excitons, arising from these loss processes and any inhomogeneous broadening, is small compared to the Rabi coupling Ω and the interactions U_X, as in Refs. [16,42,43]. (We will later also introduce an incoherent pump of the exciton states.)

BEC of polaritons in microcavities has been considered for spatially localized two-level systems within the Dicke model [44–46]. The model we study, Eq. (1), goes beyond this by allowing multiple excitons per site, and the Hubbard interaction U_X will play a key role. In the field of cold atomic gases, studies of Bose-Hubbard models coupled to cavity fields [47–49] have led to experimental breakthroughs including the Dicke phase transition [50] and supersolidity [51]. The hybridization of the inter- and intralayer excitons can be tuned through the variation of the twist angle [18], allowing for variation of the exciton-exciton interaction (via the interlayer component) and the light-matter coupling (via the intralayer component) over a wide range of parameters.

Coherent photon driving and bistability.—We start by considering a coherent drive of the cavity, as described by the term $(F\hat{a}^{\dagger}e^{-i\omega_p t} + F^{*}\hat{a}e^{i\omega_p t})$ with an amplitude F and frequency ω_p. To account for the strong exciton-exciton interactions we employ an on-site exact diagonalization for the excitons combined with a self-consistent mean-field approach for the noninteracting cavity photons, which assumes a large occupation of the photonic mode. This goes beyond an extended Gross-Pitaevskii for the compound object of exciton-photon in terms of polaritons [21]. The cavity field is given then by $\langle\hat{a}\rangle = \sqrt{N}\alpha$, the amplitude α follows from the steady-state $\alpha = (1/\Delta_c)(f + \Omega\langle x\rangle)$, where $f = F/\sqrt{N}$ and we have taken $\sum_i \langle\hat{x}_i\rangle/N = \langle x\rangle$. In addition, we introduce $\Delta_c = \Delta\omega_c + i\gamma_c/2$ with $\Delta\omega_c = \omega_p - \omega_c$, the pump detuning from the cavity. The steady state of the system is obtained by exact diagonalization of the superoperator $\mathcal{L}[\hat{\rho}] = -i[\hat{H}_{\text{local}}, \hat{\rho}] + \mathcal{D}[\hat{\rho}]$ where $\hat{H}_{\text{local}}$ is the effective exciton Hamiltonian with the cavity field α, a parameter obtained self-consistently, as explained in [52]. Here, for clarity we set $t_{ij} = 0$.

For clarity, consider first the regime of negligible saturation effects, $\Omega_{\text{sat}}/\Omega = 0$. In this case, the exciton Hamiltonian takes the form

$$\hat{H}_{\text{local}} = \hat{H}_X + \sum_i (f_X \hat{x}_i^{\dagger} + f_X^{*}\hat{x}_i), \tag{5}$$

which introduces an effective driving $f_X = (\Omega f/\Delta_c) + (\Omega^2/\Delta_c)\langle\hat{x}\rangle$. Within this regime $(\Omega_{\text{sat}} = 0)$ the density matrix can also be obtained by a self-consistent approach based on an analytical expression for the density matrix, see [52,53].

For positive pump detuning from the exciton $\Delta\omega_X = \omega_p - \omega_X > 0$, the on-site repulsion U_X can bring the transition into resonance as the density of excitons increases, leading to a sudden increase in exciton density. This effect gives rise to a bistability as a function of f/U_X. In Fig. 2(b) we show the mean exciton density for increasing f/U_X, that is when f/U_X is varied from below. On the other hand, Fig. 2(c) corresponds to the high-density hysteresis branch, that is, a decreasing f/U_X from an initial large positive f/U_X. Here the steady state remains in a high-density phase for smaller values of f/U_X compared to Fig. 2(b) indicating the hysteresis. The phase diagram consists of two monostable phases separated by a bistability. The distinctive lobular pattern in the phase diagram is determined by the n-exciton resonance,

$$(n-1) = \frac{2\Delta\omega_X}{U_X}. \tag{6}$$

Physically, the transition to the high-density phase with exciton number n can be understood as an energetic condition. When the energy of n-incoming photons equals the energy of n-interacting excitons $n\omega_p = n\omega_X + n(n-1)U_X/2$ this transition is enhanced. We illustrate our results for physically motivated parameters, by fixing $\gamma_x/U_X = 0.1$, $\gamma_c/U_X = 0.2$, $\Omega/U_X = 0.75$ and $\Delta\omega_c/U_X = -1$.

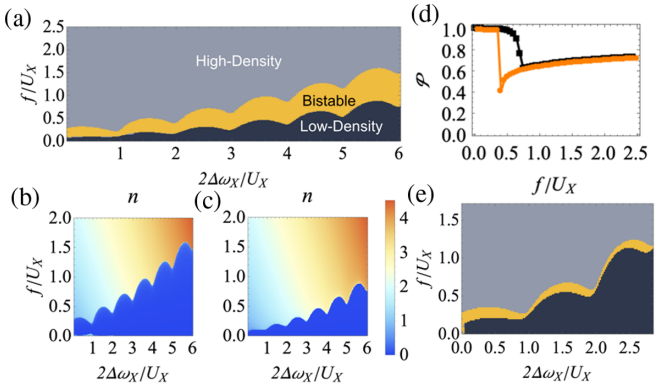

FIG. 2. (a) Stability phase diagram: black (grey) regions correspond to low (high-density) phases, separated by a bistability region (orange). Exciton number as a function of f/U_X and $\Delta\omega_X/U_X$, at $\Delta\omega_c/U_X = -1$, showing hysteresis for: (b) increasing f/U_X; and (c) decreasing f/U_X. (d) Purity of the steady state at $\Delta\omega_X/U_X = 1.2$, for the two hysteretic branches, of increasing (decreasing) f/U_X [black (orange)]. (e) Stability phase diagram showing the effects of saturation, with $\Omega_{\text{sat}} = \Omega/4$.

The bistable phase is related to a tunneling-mediated bistability, where the light-matter coupling induces effective exciton hopping through the lattice with amplitude $J_{\text{med}} \propto -\Omega^2 f/\Delta_c$. This is a second-order process, where an exciton emits a photon which is absorbed to create an exciton in a different site. A similar bistability arises within a mean-field treatment of photonic lattices, as a consequence of photon hopping between the cavities [53–56]. We emphasize that our model differs from these models of photonic cavities through the existence of both excitonic and photonic degrees of freedom. Furthermore, the parameter $\Delta k a_M \ll 1$ motivates the collective coupling of the photon field among multiple excitonic sites.

As highlighted above, for the electronic system one should also allow for saturation effects in Rabi coupling. For state-of-the-art experiments with moiré excitons the extent of the exciton wave function is of the order $r_s \approx$ 1–5 nm with typical Bohr radius of $a_B \approx 1$ nm [18,36]. Roughly, one can estimate $\Omega_{\text{sat}}/\Omega \propto (a_B/r_s)^2 \in \{0.1, 1\}$ [52]. In Fig. 2(e) we illustrate for $\Omega_{\text{sat}} = \Omega/4$ the imprints of the anharmonic light-matter coupling on the phase diagram, with all other parameters as in Fig. 2(a). For small exciton detuning, the lobular pattern respects the n-exciton resonances. Moreover, a bistable phase remainder of the phase diagram in Fig. 2(a) persists within the lobes in Fig. 2(e). The region of bistability shrinks somewhat as saturation effects increase, but the cusps remain very

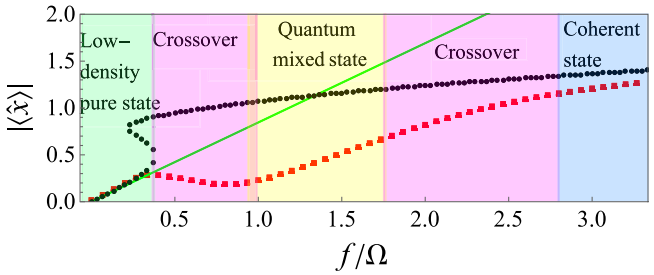

FIG. 3. Exciton amplitude $|\langle\hat{x}\rangle|$ for $\Delta\omega_X/U_X = 1.2$, and $\Delta\omega_c/U_X = 1$. We show the EGP (black dotted line), self-consistent on-site diagonalization (red dashed line), and non-interacting excitons (solid green line).

prominent. Both the bistability and the cusps associated with the n-exciton resonances remain for saturation effects of the size expected.

The results that we find arise from quantum correlations that go beyond what can be obtained in a Gross-Pitaevskii (GP) mean field theory, which is appropriate for weakly interacting excitons. In the GP method, the excitons are in a pure quantum state—albeit a coherent state with nonzero $\langle\hat{x}_i\rangle$. The states arising here are, in general, not pure. For example, the low- to high-density transition is accompanied by a change in the statistical nature of the density matrix, which evolves from a pure quantum state into a statistical mixture. Figure 2(d) shows the drop of the purity $\mathcal{P} = \mathrm{Tr}(\hat{\rho}^2)$, for $\Delta\omega_X/U_X = 1.2$ along the transition. Furthermore, for positive detuning $\Delta\omega_c > 0$, we find that the bistability predicted by EGP is inhibited, and instead the transition from the low- to high-density regime is a smooth function of f/U_X. In Fig. 3 we show $|\langle\hat{x}\rangle|$ as a function of f/U_X for $\Delta\omega_X/U_X = 1.2$, and $\Delta\omega_c/U_X = 1$. To illustrate the distinct character of the localized excitons compared to their mobile two-dimensional counterpart, we compare the solutions obtained from the master equation, the extended Gross-Pitaevskii equation (EGP) [21], and noninteracting excitons, which for weak driving intensities f/U_X, agree well. However, when the exciton density is no longer small, the failure of the EGP to capture the underlying excitation spectrum of Eq. (1) becomes evident. On the one hand, the EGP predicts always an S-shaped bistability for $\Delta\omega_X > 0$, a characteristic signature of weakly interacting polariton gases [21,57,58]. However, the steady state finds no bistable phase and is characterized instead by an abrupt but continuous drop of the coherence at $f/U_X \approx 0.25$. Figure 3 highlights that the EGP, which is sufficient for weakly interacting two-dimensional polariton gases, is no longer adequate to describe the coupling of localized excitons to light.

Incoherent pumping and lasing.—Lasers based on two-dimensional TMD materials have attracted much attention [59], in the context of photonic crystals [60], whispering gallery microcavities [61,62], polariton lasing [21,63], and trion-induced optical gain [33,64]. Interlayer excitons periodically trapped, however, open a new avenue, in which the inherited valley physics, strong interactions, and intra- and interexciton mixing make these systems ideal to realize single- and multiphoton lasers. By optically driving higher excitonic bands which quickly relax to the hybrid exciton state, it is possible to engineer driving schemes with incoherent exciton gain [65]. To represent this, we add to the exciton and cavity decay (4) the term

$$\mathcal{D}_{\mathrm{gain}}[\hat{\rho}] = \frac{\Gamma_x}{2}\sum_i [2\hat{y}_i^\dagger\hat{\rho}\hat{y}_i - \{\hat{y}_i\hat{y}_i^\dagger, \hat{\rho}\}], \tag{7}$$

which describes incoherent exciton gain at a rate Γ_x. We assume that the gain mechanism pumps the exciton number on each site up to an occupancy of at most $n_{\max}$. The jump operator is then $\hat{y}_i^\dagger \equiv \hat{x}_i\hat{P}_i$, where $\hat{P}_i$ is the projection operator on site i onto the exciton number states in the range $n_i = 0, 1, \ldots, n_{\max} - 1$. For clarity, here we take $n_{\max} = 2$. The photon energy ω is calculated self-consistently to determine the steady state, and it does not necessarily match the cavity ω_c nor the exciton ω_X energies [52]. This energy is obtained by maintaining the semi-classical treatment for the photon field. Again, we assume that only one valley exciton is driven, for example, by pumping with circular polarized light.

We find that a nontrivial state with $\alpha \neq 0$ emerges as a consequence of two processes, see Fig. 4 (inset, right): (i) Single-photon resonances, when the energy of a single photon matches the energy of the transitions $|0\rangle \to |1\rangle$ and $|1\rangle \to |2\rangle$, with $\omega \approx \omega_X$ and $\omega \approx \omega_X + U_X$ respectively, and

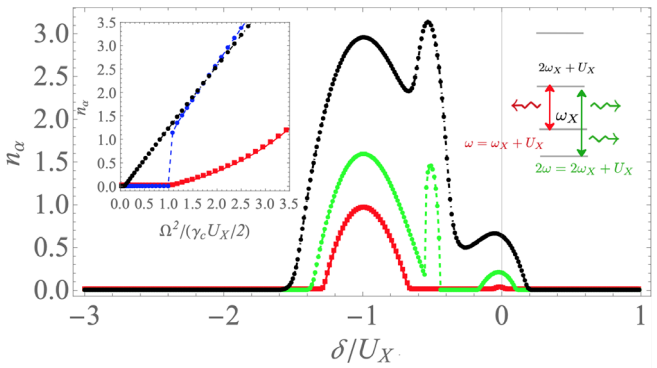

FIG. 4. Photon amplitude $n_\alpha = |\alpha|^2$ as a function of δ for $\Omega/U_X = 1/12$ (red dashed line), $\Omega/U_X = 1/8$ (green dash-dotted line), $\Omega/U_X = 1/6$ (black dash-dotted line), we fix $\Gamma_x/U = 1/10$ $\Gamma_x/\gamma_X = 6$, $\Gamma_x/\gamma_c = 3$. (inset, left) Photon amplitude as a function of $2\Omega^2/(U_X\gamma_c)$ for varying Ω. Single-particle transitions $\delta/U_X = 0$ (red dashed line) and $\delta/U_X = -1$ (black dash-dotted line) and $\delta/U_X = -1/2$ (blue dash-dotted line). (Inset, right) Sketch of the exciton level scheme and the photon transitions, the wavy red arrow illustrates the one-photon resonance $|2\rangle \to |1\rangle$, while the green wavy arrows depict a two-photon process.

(ii) two-photon resonances corresponding to the emission of two photons with $2\omega \approx 2\omega_X + U_X$.

Figure 4 shows the photon amplitude $n_\alpha = |\alpha|^2$ for several values of the light-matter coupling Ω/U_X as a function of the cavity detuning $\delta = \omega_X - \omega_c$. The single-photon resonances can be understood in terms of effective two-level systems, where the photon energy $\omega \approx \omega_X$ or $\omega \approx \omega_X + U_X$ is resonant with the one-particle transitions $|0\rangle \rightarrow |1\rangle$ and $|1\rangle \rightarrow |2\rangle$, respectively. The injection of excitons induces population inversion, that is $\rho_{22} > \rho_{11} > \rho_{00}$, leading to an enhanced photon amplitude for the $|2\rangle \rightarrow |1\rangle$ transition, compared to the one-photon transition with energy $\omega_c = \omega_X$. Interpreting the single-photon transitions in terms of effective two-level systems, the nontrivial solutions arise beyond a critical light-matter coupling $\Omega_c = (\gamma_x + \Gamma_x)\sqrt{\{\gamma_c/[4(\Gamma_x - \gamma_x)]\}}$, see Supplemental Material [52].

Emission of photon pairs is promoted at the two-photon resonance, that is, $\delta/U_X = -1/2$, due to the strong exciton interactions: the single- and multiphoton resonances are well-separated in energy, and can be clearly distinguished in Fig. 4. Inspired by the studies on lasers based on two-photon gain in three-level atoms [22–25], we introduce an effective two-photon coupling $g_2 = \Omega^2/\Delta$, where $\Delta = U_X/2$ is fixed by the discrete levels of the excitonic spectrum. In Fig. 4 (inset, left) we plot the amplitude of the cavity field as a function of g_2/γ_c at the single-particle transitions $\delta/U_X = 0$ (red) and $\delta/U_X = -1$ (black) and at the two-photon resonance $\delta/U_X = -1/2$ (blue). The sudden appearance of two-photon lasing can be also understood in terms of effective laser rate equations, which predict a photon number that discontinuously jumps to $n_\alpha \approx 2\Gamma_x/(5\gamma_c)$, with a two-photon stimulated rate of $A_2 \propto g_2^2/\Gamma_x$, see [52]. Here, saturation effects for $\Omega_s = \Omega/4$ lead only to quantitative corrections, leaving our main conclusions valid.

Conclusions.—We have demonstrated that for moiré materials, the competition between exciton interaction, saturation effects, nonequilibrium features, and strong light-matter interactions, leads to a rich phase diagram with no counterpart in conventional two-dimensional polariton gases. The expected optical bistabilities could be detected by measuring the transmitted spectrum in a similar fashion to polariton gases [41,66,67]. Detection of the cusps in the bistability would allow a direct measurement of the local Hubbard interaction of excitons. These materials also permit the incoherent drive of excitons, for example, by optically driving higher excitonic bands which quickly relax to the interlayer exciton state [65]. Our work opens up the door for studies on the role of free carriers in moiré lattices [43,68], effects arising from the parabolic dispersion of the photons [69–71], the longitudinal-transverse splitting of the excitons [42], and physics beyond our mean-field treatment for the cavity photons.

Data supporting this publication are available in the Apollo repository [72].

We are grateful to Mete Atatüre, Jeremy Baumberg, and Benjamin Remez for helpful discussions. This work was supported by EPSRC Grants No. EP/P009565/1 and No. EP/P034616/1, and by a Simons Investigator Award.

*Present Address: Departamento de Física Química, Instituto de Física, Universidad Nacional Autónoma de México, Apartado Postal 20-364, Ciudad de México C.P. 01000, Mexico.

[1] S. Manzeli, D. Ovchinnikov, D. Pasquier, O. V. Yazyev, and A. Kis, 2d transition metal dichalcogenides, Nat. Rev. Mater. **2**, 17033 (2017).
[2] Y. Tang, L. Li, T. Li, Y. Xu, S. Liu, K. Barmak, K. Watanabe, T. Taniguchi, A. H. MacDonald, J. Shan, and K. F. Mak, Simulation of hubbard model physics in WSe2/WS2 moiré superlattices, Nature (London) **579**, 353 (2020).
[3] D. M. Kennes, M. Claassen, L. Xian, A. Georges, A. J. Millis, J. Hone, C. R. Dean, D. N. Basov, A. N. Pasupathy, and A. Rubio, Moiré heterostructures as a condensed-matter quantum simulator, Nat. Phys. **17**, 155 (2021).
[4] H. Baek, M. Brotons-Gisbert, Z. X. Koong, A. Campbell, M. Rambach, K. Watanabe, T. Taniguchi, and B. D. Gerardot, Highly energy-tunable quantum light from moiré-trapped excitons, Sci. Adv. **6** (2020).
[5] H. Yu and W. Yao, Electrically tunable topological transport of moiré polaritons, Sci. Bull. **65**, 1555 (2020).
[6] Y. Liu, N. O. Weiss, X. Duan, H.-C. Cheng, Y. Huang, and X. Duan, Van der waals heterostructures and devices, Nat. Rev. Mater. **1**, 16042 (2016).
[7] J. R. Schaibley, H. Yu, G. Clark, P. Rivera, J. S. Ross, K. L. Seyler, W. Yao, and X. Xu, Valleytronics in 2d materials, Nat. Rev. Mater. **1**, 16055 (2016).
[8] A. Rasmita and W.-b. Gao, Opto-valleytronics in the 2d van der waals heterostructure, Nano Res. **14**, 1901 (2021).
[9] Y. Tang, J. Gu, S. Liu, K. Watanabe, T. Taniguchi, J. Hone, K. F. Mak, and J. Shan, Tuning layer-hybridized moiré excitons by the quantum-confined stark effect, Nat. Nanotechnol. **16**, 52 (2021).
[10] M. Förg, A. S. Baimuratov, S. Y. Kruchinin, I. A. Vovk, J. Scherzer, J. Förste, V. Funk, K. Watanabe, T. Taniguchi, and A. Högele, Moiréexcitons in mose2-WSe2 heterobilayers and heterotrilayers, Nat. Commun. **12**, 1656 (2021).
[11] W.-T. Hsu, B.-H. Lin, L.-S. Lu, M.-H. Lee, M.-W. Chu, L.-J. Li, W. Yao, W.-H. Chang, and C.-K. Shih, Tailoring excitonic states of van der waals bilayers through stacking configuration, band alignment, and valley spin, Sci. Adv. **5** (2019).
[12] J. Jung, A. Raoux, Z. Qiao, and A. H. MacDonald, *Ab initio* theory of moiré superlattice bands in layered two-dimensional materials, Phys. Rev. B **89**, 205414 (2014).
[13] C. Zhang, C.-P. Chuu, X. Ren, M.-Y. Li, L.-J. Li, C. Jin, M.-Y. Chou, and C.-K. Shih, Interlayer couplings, moiré patterns, and 2d electronic superlattices in MoS2/WSe2 hetero-bilayers, Sci. Adv. **3** (2017).
[14] S. Ulstrup, R. J. Koch, S. Singh, K. M. McCreary, B. T. Jonker, J. T. Robinson, C. Jozwiak, E. Rotenberg,

A. Bostwick, J. Katoch, and J. A. Miwa, Direct observation of minibands in a twisted graphene/ws2 bilayer, Sci. Adv. **6** (2020).
[15] K. Tran, J. Choi, and A. Singh, Moiré and beyond in transition metal dichalcogenide twisted bilayers, 2D Mater. **8**, 022002 (2021).
[16] Y. Jiang, S. Chen, W. Zheng, B. Zheng, and A. Pan, Interlayer exciton formation, relaxation, and transport in TMD van der waals heterostructures, Light Sci. Appl. **10**, 72 (2021).
[17] A. Tartakovskii, Excitons in 2d heterostructures, Nat. Rev. Phys. **2**, 8 (2020).
[18] E. M. Alexeev, D. A. Ruiz-Tijerina, M. Danovich, M. J. Hamer, D. J. Terry, P. K. Nayak, S. Ahn, S. Pak, J. Lee, J. I. Sohn, M. R. Molas, M. Koperski, K. Watanabe, T. Taniguchi, K. S. Novoselov, R. V. Gorbachev, H. S. Shin, V. I. Fal'ko, and A. I. Tartakovskii, Resonantly hybridized excitons in moiré superlattices in van der waals heterostructures, Nature (London) **567**, 81 (2019).
[19] D. A. Ruiz-Tijerina and V. I. Fal'ko, Interlayer hybridization and moiré superlattice minibands for electrons and excitons in heterobilayers of transition-metal dichalcogenides, Phys. Rev. B **99**, 125424 (2019).
[20] Y. Shimazaki, I. Schwartz, K. Watanabe, T. Taniguchi, M. Kroner, and A. Imamoğlu, Strongly correlated electrons and hybrid excitons in a moiré heterostructure, Nature (London) **580**, 472 (2020).
[21] I. Carusotto and C. Ciuti, Quantum fluids of light, Rev. Mod. Phys. **85**, 299 (2013).
[22] M. Brune, J. M. Raimond, and S. Haroche, Theory of the Rydberg-atom two-photon micromaser, Phys. Rev. A **35**, 154 (1987).
[23] L. Davidovich, J. M. Raimond, M. Brune, and S. Haroche, Quantum theory of a two-photon micromaser, Phys. Rev. A **36**, 3771 (1987).
[24] M. Lewenstein, Y. Zhu, and T. W. Mossberg, Two-Photon Gain and Lasing in Strongly Driven Two-Level Atoms, Phys. Rev. Lett. **64**, 3131 (1990).
[25] M. Orszag, L. Roa, and R. Ramírez, Generation of pure states in a two-photon micromaser: Effects of finite detuning and cavity losses, Phys. Rev. A **48**, 4648 (1993).
[26] J. Kasprzak, M. Richard, S. Kundermann, A. Baas, P. Jeambrun, J. M. J. Keeling, F. M. Marchetti, M. H. Szymańska, R. André, J. L. Staehli, V. Savona, P. B. Littlewood, B. Deveaud, and L. S. Dang, Bose–Einstein condensation of exciton polaritons, Nature (London) **443**, 409 (2006).
[27] H. Deng, H. Haug, and Y. Yamamoto, Exciton-polariton bose-einstein condensation, Rev. Mod. Phys. **82**, 1489 (2010).
[28] A. Amo, J. Lefrère, S. Pigeon, C. Adrados, C. Ciuti, I. Carusotto, R. Houdré, E. Giacobino, and A. Bramati, Superfluidity of polaritons in semiconductor microcavities, Nat. Phys. **5**, 805 (2009).
[29] L. Dominici, R. Carretero-González, A. Gianfrate, J. Cuevas-Maraver, A. S. Rodrigues, D. J. Frantzeskakis, G. Lerario, D. Ballarini, M. De Giorgi, G. Gigli, P. G. Kevrekidis, and D. Sanvitto, Interactions and scattering of quantum vortices in a polariton fluid, Nat. Commun. **9**, 1467 (2018).
[30] N. Takemura, S. Trebaol, M. Wouters, M. T. Portella-Oberli, and B. Deveaud, Polaritonic feshbach resonance, Nat. Phys. **10**, 500 (2014).
[31] M. Sidler, P. Back, O. Cotlet, A. Srivastava, T. Fink, M. Kroner, E. Demler, and A. Imamoglu, Fermi polaron-polaritons in charge-tunable atomically thin semiconductors, Nat. Phys. **13**, 255 (2017).
[32] R. P. A. Emmanuele, M. Sich, O. Kyriienko, V. Shahnazaryan, F. Withers, A. Catanzaro, P. M. Walker, F. A. Benimetskiy, M. S. Skolnick, A. I. Tartakovskii, I. A. Shelykh, and D. N. Krizhanovskii, Highly nonlinear trion-polaritons in a monolayer semiconductor, Nat. Commun. **11**, 3589 (2020).
[33] L. B. Tan, O. Cotlet, A. Bergschneider, R. Schmidt, P. Back, Y. Shimazaki, M. Kroner, and A. m. c. İmamoğlu, Interacting Polaron-Polaritons, Phys. Rev. X **10**, 021011 (2020).
[34] V. Shahnazaryan, V. K. Kozin, I. A. Shelykh, I. V. Iorsh, and O. Kyriienko, Tunable optical nonlinearity for transition metal dichalcogenide polaritons dressed by a fermi sea, Phys. Rev. B **102**, 115310 (2020).
[35] A. Camacho-Guardian, M. A. Bastarrachea-Magnani, and G. M. Bruun, Mediated Interactions and Photon Bound States in an Exciton-Polariton Mixture, Phys. Rev. Lett. **126**, 017401 (2021).
[36] L. Zhang, F. Wu, S. Hou, Z. Zhang, Y.-H. Chou, K. Watanabe, T. Taniguchi, S. R. Forrest, and H. Deng, Van der waals heterostructure polaritons with moiré-induced nonlinearity, Nature (London) **591**, 61 (2021).
[37] M. Combescot, M. A. Dupertuis, and O. Betbeder-Matibet, Polariton-polariton scattering: Exact results through a novel approach, Europhys. Lett. **79**, 17001 (2007).
[38] J. Levinsen, G. Li, and M. M. Parish, Microscopic description of exciton-polaritons in microcavities, Phys. Rev. Research **1**, 033120 (2019).
[39] S. Schmitt-Rink, D. S. Chemla, and D. A. B. Miller, Theory of transient excitonic optical nonlinearities in semiconductor quantum-well structures, Phys. Rev. B **32**, 6601 (1985).
[40] C. Ciuti, P. Schwendimann, B. Deveaud, and A. Quattropani, Theory of the angle-resonant polariton amplifier, Phys. Rev. B **62**, R4825 (2000).
[41] A. Baas, J. P. Karr, H. Eleuch, and E. Giacobino, Optical bistability in semiconductor microcavities, Phys. Rev. A **69**, 023809 (2004).
[42] K. L. Seyler, P. Rivera, H. Yu, N. P. Wilson, E. L. Ray, D. G. Mandrus, J. Yan, W. Yao, and X. Xu, Signatures of moiré-trapped valley excitons in MoSe2/WSe2 heterobilayers, Nature (London) **567**, 66 (2019).
[43] E. Liu, E. Barré, J. van Baren, M. Wilson, T. Taniguchi, K. Watanabe, Y.-T. Cui, N. M. Gabor, T. F. Heinz, Y.-C. Chang, and C. H. Lui, Signatures of moiré trions in WSe2/MoSe2 heterobilayers, Nature (London) **594**, 46 (2021).
[44] P. R. Eastham and P. B. Littlewood, Bose condensation of cavity polaritons beyond the linear regime: The thermal equilibrium of a model microcavity, Phys. Rev. B **64**, 235101 (2001).
[45] M. H. Szymanska, P. B. Littlewood, and B. D. Simons, Polariton condensation and lasing in optical microcavities: The decoherence-driven crossover, Phys. Rev. A **68**, 013818 (2003).

[46] J. Keeling, P. R. Eastham, M. H. Szymanska, and P. B. Littlewood, Polariton Condensation with Localized Excitons and Propagating Photons, Phys. Rev. Lett. **93**, 226403 (2004).
[47] F. Brennecke, T. Donner, S. Ritter, T. Bourdel, M. Köhl, and T. Esslinger, Cavity qed with a Bose–Einstein condensate, Nature (London) **450**, 268 (2007).
[48] H. Ritsch, P. Domokos, F. Brennecke, and T. Esslinger, Cold atoms in cavity-generated dynamical optical potentials, Rev. Mod. Phys. **85**, 553 (2013).
[49] I. B. Mekhov and H. Ritsch, Quantum optics with ultracold quantum gases: Towards the full quantum regime of the light-matter interaction, J. Phys. B Atom. Mol. Phys. **45**, 102001 (2012).
[50] K. Baumann, C. Guerlin, F. Brennecke, and T. Esslinger, Dicke quantum phase transition with a superfluid gas in an optical cavity, Nature (London) **464**, 1301 (2010).
[51] J. Léonard, A. Morales, P. Zupancic, T. Esslinger, and T. Donner, Supersolid formation in a quantum gas breaking a continuous translational symmetry, Nature (London) **543**, 87 (2017).
[52] See Supplemental Material at http://link.aps.org/supplemental/10.1103/PhysRevLett.128.207401 for details.
[53] P. D. Drummond and D. F. Walls, Quantum theory of optical bistability. I. Nonlinear polarisability model, J. Phys. A **13**, 725 (1980).
[54] A. Le Boité, G. Orso, and C. Ciuti, Steady-State Phases and Tunneling-Induced Instabilities in the Driven Dissipative Bose-Hubbard Model, Phys. Rev. Lett. **110**, 233601 (2013).
[55] A. Le Boité, G. Orso, and C. Ciuti, Bose-hubbard model: Relation between driven-dissipative steady states and equilibrium quantum phases, Phys. Rev. A **90**, 063821 (2014).
[56] M. Biondi, G. Blatter, H. E. Türeci, and S. Schmidt, Nonequilibrium gas-liquid transition in the driven-dissipative photonic lattice, Phys. Rev. A **96**, 043809 (2017).
[57] C. Ciuti and I. Carusotto, Quantum fluid effects and parametric instabilities in microcavities, Phys. Status Solidi (b) **242**, 2224 (2005).
[58] O. Kyriienko, E. A. Ostrovskaya, O. A. Egorov, I. A. Shelykh, and T. C. H. Liew, Bistability in microcavities with incoherent optical or electrical excitation, Phys. Rev. B **90**, 125407 (2014).
[59] W. Wen, L. Wu, and T. Yu, Excitonic lasers in atomically thin 2d semiconductors, ACS Mater. Lett. **2**, 1328 (2020).
[60] S. Wu, S. Buckley, J. R. Schaibley, L. Feng, J. Yan, D. G. Mandrus, F. Hatami, W. Yao, J. Vučković, A. Majumdar, and X. Xu, Monolayer semiconductor nanocavity lasers with ultralow thresholds, Nature (London) **520**, 69 (2015).
[61] Y. Ye, Z. J. Wong, X. Lu, X. Ni, H. Zhu, X. Chen, Y. Wang, and X. Zhang, Monolayer excitonic laser, Nat. Photonics **9**, 733 (2015).
[62] O. Salehzadeh, M. Djavid, N. H. Tran, I. Shih, and Z. Mi, Optically pumped two-dimensional mos2 lasers operating at room-temperature, Nano Lett. **15**, 5302 (2015).
[63] H. Shan, L. Lackner, B. Han, E. Sedov, C. Rupprecht, H. Knopf, F. Eilenberger, K. Yumigeta, K. Watanabe, T. Taniguchi, S. Klembt, S. Höfling, A. V. Kavokin, S. Tongay, C. Schneider, and C. Antón-Solanas, Coherent light emission of exciton-polaritons in an atomically thin crystal at room temperature, Nat. Commun. **12**, 6406 (2021).
[64] T. Wasak, F. Pientka, and F. Piazza, Fermi polaron laser in two-dimensional semiconductors, arXiv:2103.14040.
[65] E. Y. Paik, L. Zhang, G. W. Burg, R. Gogna, E. Tutuc, and H. Deng, Interlayer exciton laser of extended spatial coherence in atomically thin heterostructures, Nature (London) **576**, 80 (2019).
[66] T. K. Paraïso, M. Wouters, Y. Léger, F. Morier-Genoud, and B. Deveaud-Plédran, Multistability of a coherent spin ensemble in a semiconductor microcavity, Nat. Mater. **9**, 655 (2010).
[67] C. Ouellet-Plamondon, G. Sallen, F. Morier-Genoud, D. Y. Oberli, M. T. Portella-Oberli, and B. Deveaud, Reservoir-induced decoherence of resonantly excited confined polaritons, Phys. Rev. B **95**, 085302 (2017).
[68] X. Wang, J. Zhu, K. L. Seyler, P. Rivera, H. Zheng, Y. Wang, M. He, T. Taniguchi, K. Watanabe, J. Yan, D. G. Mandrus, D. R. Gamelin, W. Yao, and X. Xu, Moirétrions in MoSe2/WSe2 heterobilayers, Nat. Nanotechnol. **16**, 1208 (2021).
[69] A. Kavokin, G. Malpuech, and M. Glazov, Optical Spin Hall Effect, Phys. Rev. Lett. **95**, 136601 (2005).
[70] C. Leyder, M. Romanelli, J. P. Karr, E. Giacobino, T. C. H. Liew, M. M. Glazov, A. V. Kavokin, G. Malpuech, and A. Bramati, Observation of the optical spin hall effect, Nat. Phys. **3**, 628 (2007).
[71] S. Dufferwiel, F. Li, E. Cancellieri, L. Giriunas, A. A. P. Trichet, D. M. Whittaker, P. M. Walker, F. Fras, E. Clarke, J. M. Smith, M. S. Skolnick, and D. N. Krizhanovskii, Spin Textures of Exciton-Polaritons in a Tunable Microcavity with Large TE-TM Splitting, Phys. Rev. Lett. **115**, 246401 (2015).
[72] N. Cooper and A. Camacho-Guardian, Data moiré nonlinearities (2022) 10.17863/CAM.83866.